Membrane Bilayer Balance and Erythrocyte Shape: A Quantitative Assessment†

James E. Ferrell, Jr., Kong-Joo Lee, and Wray H. Huestis*
Department of Chemistry, Stanford University, Stanford, California 94305
Received June 18, 1984; Revised Manuscript Received November 6, 1984

ABSTRACT: When human erythrocytes are incubated with certain phospholipids, the cells become spiculate echinocytes, resembling red cells subjected to metabolic starvation or Ca^{2+} loading. The present study examines (1) the mode of binding of saturated phosphatidylcholines and egg lysophosphatidylcholine to erythrocytes and (2) the quantitative relationship between phospholipid incorporation and red cell shape. We find that the phospholipids studied become intercalated into erythrocyte membranes, not simply adsorbed to the cell surface. Spin-labeling and radiolabeling data show that the incorporation of $(4 \pm 1) \times 10^6$ molecules of exogenous phosphatidylcholine per cell converts discocytes to stage 3 echinocytes with about 35 conical spicules. This amount of lipid incorporation is estimated to expand the red cell membrane outer monolayer by 1.7% ± 0.6%. Calculations of the inner and outer monolayer surface areas of model discocytes and stage 3 echinocytes yield an estimated difference of 0.7% ± 0.2%.

The normal biconcave disk shape of the human erythrocyte can be altered by Ca^{2+} loading (White, 1974), by metabolic depletion (Nakao et al., 1960), or by incubation with certain amphipathic compounds (Sheetz & Singer, 1974). Some amphipaths, crenators, induce a shape change called echinocytosis. At low concentrations, crenators cause the normally smooth contour of the erythrocyte to develop broad convexities which narrow into spikes and grow finer and more numerous as the amount of bound amphipath increases. High concentrations of crenators cause the tips of the spikes to pinch off, forming membrane buds, until the cell is left a smooth spheroechinocyte. Still higher concentrations cause the spheroechinocyte to lyse.

Another class of amphipaths reverses the effects of crenators and causes stomatocytosis. Erythrocytes exposed to low concentration of these agents assume a cupped shape. With increasing amphipath concentrations, the membrane develops invaginations which become more numerous and break off as endocytotic vesicles. Eventually, the cell becomes roughly spherical; finally, the spherostomatocyte lyses.

Sheetz & Singer (1974) first proposed that these shape changes arise from differential expansion of the cell membrane monolayers (the "bilayer couple hypothesis"). Echinocytogenic amphipaths were thought to intercalate in the cell membrane and remain kinetically trapped in the outer monolayer (e.g., lysophosphatidylcholine) or to equilibrate preferentially into the outer leaflet (e.g., barbiturates). The cell would then accommodate its expanded outer leaflet by crenating. Cup formers like chlorpromazine were thought to accumulate in the inner monolayer, presumably because of energetically favorable interactions with the acidic phospholipids of that leaflet. The resulting expansion of the inner leaflet would then produce stomatocytosis. The demonstrable binding of amphipaths such as phospholipids to red cells was consistent with this model (Bouma et al., 1977).

The bilayer couple hypothesis explained the morphological effects of a wide variety of amphipaths and successfully predicted the effects of many others (Fujii et al., 1979). However, recently Conrad & Singer (1981) cast serious doubts on a fundamental assumption underlying the bilayer couple hypothesis. Using a new filtration method to measure the partitioning of amphipaths, they concluded that although such compounds bind to synthetic membranes, they do not intercalate into erythrocyte membranes to any appreciable extent. Conrad and Singer inferred that biological membranes, in contrast to synthetic membranes, must have high internal pressure that prevents the insertion of exogenous molecules. They suggested that the shape changes caused by amphipaths might be related to the tendency of these compounds to form micelles near the cell surface. These conclusions are difficult to reconcile with the apparent insertion of fluorescent compounds into lipid domains of erythrocyte membranes (Matayoshi, 1980; Chalpin & Kleinfeld, 1983).

We have examined the shape change that occurs after erythrocytes are depleted of ATP (Ferrell & Huestis, 1984), a process apparently similar to amphipath-induced crenation. Metabolic crenation was found to be accompanied by the degradation of two inner monolayer phospholipids, phosphatidylinositol 4,5-bisphosphate and phosphatidic acid. The former is converted to phosphatidylinositol, a smaller, less highly charged molecule, and the latter to diacylglycerol, a neutral lipid that should equilibrate across the bilayer (Allan et al., 1978). In the context of the bilayer couple hypothesis, it seemed plausible that the loss of inner leaflet area arising from these lipid conversions (estimated to be about 0.65%) could account for the shape change. We proposed that a related process, Ca^{2+}-induced crenation, also arises from bilayer imbalance attendant to degradation of phosphatidylinositol 4-phosphate and phosphatidylinositol 4,5-bisphosphate, but by a different pathway: the Ca^{2+}-dependent phospholipase C described by Allan, Michell, and co-workers (Allan et al., 1976; Allan & Michell, 1978; Allan & Thomas, 1981).

The present study was designed to test the quantitative aspects of these hypotheses. The objectives were to determine whether amphipaths intercalate into erythrocyte membranes (as assumed by the bilayer couple hypothesis) or become associated with cells in some other manner [as suggested by Conrad & Singer (1981)], to measure the binding of phosphatidylcholine (PC)[1] and lysophosphatidylcholine (lyso-PC) to erythrocytes, and to use the known cross-sectional areas of these molecules to assess the relationship between outer

† This work was supported by grants from the National Institutes of Health (HL 23787) and the American Heart Association (Grant in Aid 80990).

[1] Abbreviations: DLPC, dilauroylphosphatidylcholine; DMPC, dimyristoylphosphatidylcholine; DOPC, dioleoylphosphatidylcholine; HCT, hematocrit; lyso-PC, lysophosphatidylcholine; PC, phosphatidylcholine; spin PC, 1-palmitoyl-2-[9-(4,4-dimethyloxazolidine-*N*-oxyl)stearoyl]-phosphatidylcholine; TLC, thin-layer chromatography; EPR, electron paramagnetic resonance.

0006-2960/85/0424-2849$01.50/0

monolayer expansion and erythrocyte shape. Finally, inner and outer leaflet surface areas were calculated for geometrical models of echinocytes. Our findings support the bilayer couple hypothesis and show that about 1.3% expansion of the outer monolayer (or contraction of the inner monolayer) can account for the extent of echinocytosis seen in metabolic crenation.

Materials and Methods

Blood was obtained by venipuncture from healthy adult volunteers. Erythrocytes were separated by centrifugation and washed 3 times with 4 volumes of 150 mM NaCl and once with 138 mM NaCl, 5 mM KCl, 6.1 mM Na_2HPO_4, 1.4 mM NaH_2PO_4, 1 mM $MgSO_4$, and 5 mM glucose, pH 7.4 ($NaCl/P_i$). Cells were used within 6 h of being drawn. For incubations longer than 5 h, penicillin G (100 μg/mL) and tobramycin (40 μg/mL) were added to retard bacterial growth. Unless otherwise noted, incubations were carried out at 37 °C in capped plastic tubes.

Lipids were purchased from Sigma [dimyristoyl-PC (DMPC), dilauroyl-PC (DLPC), dioleoyl-PC (DOPC), cholesterol, and egg lyso-PC, assayed by Sigma to contain 65% palmitoyl, 30% stearoyl, and 3% oleoyl acyl chains] and Avanti Biochemicals [DLPC and 1-palmitoyl-2-[9-(4,4-dimethyloxazolidine-*N*-oxyl)stearoyl]phosphatidylcholine (spin PC)]. Limit vesicles (or, in the case of lyso-PC, micelles) were prepared by suspending lipid in $NaCl/P_i$ and sonicating the suspension to clarity in a bath sonicator. DLPC, DMPC, and DPPC vesicles prepared by this method were shown to be unilamellar and monodisperse by Sephacryl S-1000 column chromatography [see also Bouma et al. (1977)].

[^{14}C]DMPC was synthesized from DMPE (Avanti) and methyl iodide (Aldrich) plus [^{14}C]methyl iodide (ICN) as described (Stockton et al., 1974). The product was purified by thin-layer chromatography (TLC) on silica gel G plates (Analtech; 250-μm layer, 5 × 20 cm, not activated) in 13:8:2 (v/v) chloroform/methanol/water. [^{3}H]Cholesteryl oleate was purchased from New England Nuclear.

Vesicles were incubated with cells (lengths of incubation, hematocrits, and concentrations as indicated in figure legends), and the cell and vesicle fractions were then separated. Mixtures of cells and DOPC or spin PC vesicles were separated by centrifugation for 3 min at 8800*g*. The cell pellet was washed once with 20 volumes of 150 mM NaCl and pelleted again. This procedure did not adequately separate DMPC vesicles from cells. During incubation with cells, DMPC vesicles appeared to aggregate: a white layer largely devoid of cells would pellet on top of the cells. This copelleting was avoided by layering the suspensions on a cushion of 150 mM NaCl/42% (w/v) sucrose and then centrifuging for 3 min at 8800*g*. The cells pelleted, while the supernatant and vesicle aggregates remained on top of the cushion. Incorporation of [^{14}C]DMPC into the cell pellet was measured by scintillation counting after bleaching with 30% H_2O_2 (10 μL/μL of cell pellet).

EPR spectra of spin-labeled cells and vesicles (20 μL) were taken at 37 °C, 9.15 GHz, and 100 mW with a Varian E-112 spectrometer. The spectra were digitized, and their absorption intensities were determined by double integration.

Supernatant lipids were extracted in 18 volumes of 2:1 (v/v) methanol/chloroform followed by 6 volumes of water and 6 volumes of chloroform. The organic phase was blown dry under a stream of nitrogen and analyzed by TLC on silica gel G plates (250-μm coating, Analtech) developed in 65:60:2.5:2.5 chloroform/methanol/water/concentrated NH_3 (typical R_f values: lyso-PC, 0.05; sphingomyelin, 0.11; PC and spin PC, 0.17; PS, 0.21; PE, 0.57; cholesterol, 0.89). Spin PC was separated from PC on Whatman reversed-phase plates developed in 45:45:4 chloroform/methanol/water (R_f values: egg PC, 0.24; spin PC, 0.31; cholesterol, 0.56). Cholesterol was assayed by the methanol of Zlatkis et al. (1953).

Rapid ATP depletion was induced by incubating cells at 20% hematocrit (HCT) with $NaCl/P_i$ plus 10 mM inosine and 6 mM iodoacetamide (Lew, 1971).

Cell morphology was assessed by light microscopy as described (Ferrell & Huestis, 1984) and graded on a scale of 0–5 based on the nomenclature of Bessis (1973). The grading scale was as follows: discocytes, 0; stage 1 echinocytes, discoid with up to 20 broad bumps and a detectable biconcavity, 1; stage 2 echinocytes, ovoid with up to 40 spikes and no biconcavity, 2; stage 3 echinocytes, spherical with 30–50 conical spikes, 3; stage 1 spheroechinocytes, spherical with about 50 threadlike spikes, 4; stage 2 spheroechinocytes, smooth spheres by light microscopy, 5. The average score for a field of 100 cells was called its morphological index. Some cell samples were examined by scanning electron microscopy as described (Ferrell & Huestis, 1984).

Results

Experimental Results. Ideally, a probe of outer monolayer expansion should possess four properties: (1) its cross-sectional area should be known; (2) its association with the cell membrane should be amenable to characterization and quantitation; (3) it should not extract membrane components from the cell; and (4) its flip-flop to the inner leaflet of the cell should be slow compared to its rate of incorporation. We elected to study three phosphatidylcholines (DLPC, DMPC, and spin PC) and egg lyso-PC, each of which meets some or all of these criteria.

Mode of Binding. When lipid vesicles are incubated with cells, lipid disappears from the supernatant and the cells change shape (Figure 1). If the bilayer couple hypothesis is correct, the shape change arises from lipid molecules intercalating into the outer leaflet of the cell membrane. On the other hand, if exogenous lipid molecules are excluded from the membrane by high internal pressure, then the apparent binding of lipid to the cells might reflect adsorption of entire vesicles or individual lipid molecules without incorporation into the membrane. These possibilities were examined with spin PC. The EPR spectrum of this molecule is sensitive to its freedom of motion and the proximity of other spin PC molecules. When low concentrations of spin PC are cosonicated with DMPC, the usual nitroxide triplet spectrum results [Figure 2a; see also Devaux et al. (1973)]. However, in vesicles composed solely of spin PC, spin exchange broadens the spectrum, resulting in an apparent singlet (Figure 2b). Pure spin PC vesicles (at 46–464 μmol/L of supernatant) were incubated with red cells at 50% HCT for 2 h, and cells were separated from supernatants by centrifugation. Vesicles simply adhering to cells or trapped in the cell pellet should exhibit a broad "singlet" spectrum as in Figure 2b. Individual spin PC molecules loosely associated with but not intercalated into the cells would give rise to a motionally unhindered triplet spectrum as in Figure 2a. If, however, the spin PC molecules were inserted into the cell membrane, an anisotropic triplet spectrum with a broad upfield peak would result. As shown in Figure 2c, the spectrum of the cell pellet was a highly anisotropic triplet. The cell-associated spin PC was resistant to brief treatments with the reducing agent ascorbic acid. The triplet character of the spectrum implies that the spin PC molecules in the cell pellet have been diluted at least 1:10 by non-spin-labeled neighboring molecules (Devaux et al., 1973), and the anisotropic character indicates that the molecules are rotationally hindered. The spectrum of the supernatant retained the broad singlet char-

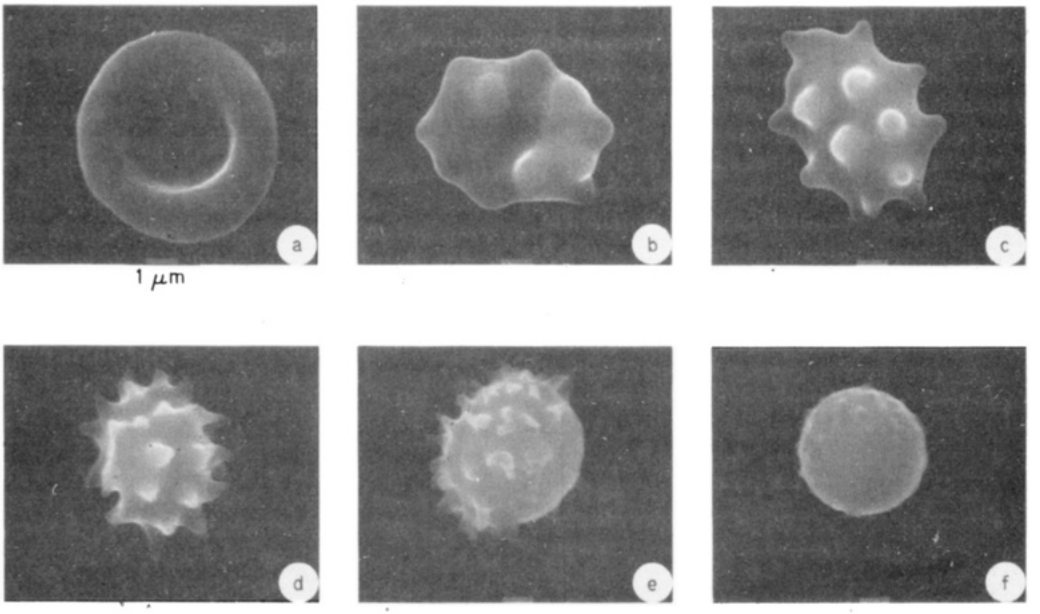

FIGURE 1: Scanning electron micrographs of erythrocytes treated with DMPC or DLPC vesicles, yielding discocytes (a) and stage 1–5 echinocytes (b–f). Estimated lipid incorporation, on the basis of tracers (see Figure 7), was 0, 30, 55, 80, 120, and 250 μmol/L of cells, respectively.

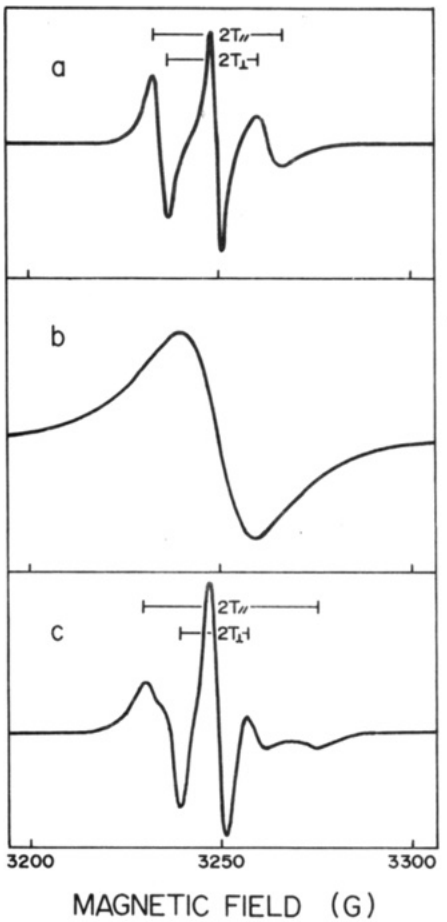

FIGURE 2: EPR spectra of (a) vesicles composed of DMPC and spin PC, 100:1 (w/w), (b) pure spin PC vesicles, and (c) erythrocytes after incubation with spin PC vesicles. The order parameters are $S = 0.18$ (a) and 0.54 (c).

acter of pure spin PC vesicles.

As a second test, DMPC vesicles labeled with [^{14}C]DMPC and [^{3}H]cholesteryl oleate (a nontransferable lipid marker) were incubated with erythrocytes. As shown in Figure 3, [^{14}C]DMPC became associated with the cells but [^{3}H]-cholesteryl oleate did not.

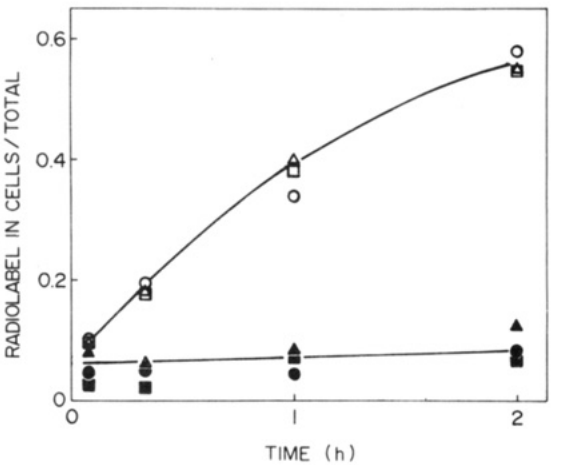

FIGURE 3: Transfer of [^{14}C]DMPC (○, □, △) and [^{3}H]cholesteryl oleate (●, ■, ▲) from DMPC vesicles [(△, ▲) 14.4 μmol/L of supernatant; (□, ■) 28.7 μmol/L of supernatant; (○, ●) 71.8 μmol/L of supernatant] to erythrocytes (50% HCT).

The kinetics of [^{14}C]DMPC transfer from cells to vesicles can also be used to test the mode of DMPC–cell association. As shown in the following paper (Ferrell et al., 1985), DMPC transfers between membranes by dissociating as a monomer from the donor membrane, diffusing through the aqueous phase, and then associating with an acceptor membrane. Present evidence suggests that if DMPC intercalates in erythrocyte membranes, the rate coefficient for dissociation of DMPC from an erythrocyte should be similar to, and probably no larger than, the rate coefficient for dissociation of DMPC from a vesicle. For example, the rate of cholesterol dissociation from red cells and egg lyso-PC vesicles is roughly equal (Lange et al., 1983), as is the rate of DMPC dissociation from DMPC or DPPC vesicles (Ferrell et al., 1985). If the cell-associated DMPC is not intercalated in the membrane but more superficially bound, its dissociation should be much more rapid.

Cells were labeled with trace amounts of [^{14}C]DMPC. The labeled cells [morphological index (MI) = +0.1] were washed and then reincubated with vesicles composed of DOPC. Under the conditions employed, negligible amounts of DOPC are transferred to the cells; instead, the DOPC vesicles act as

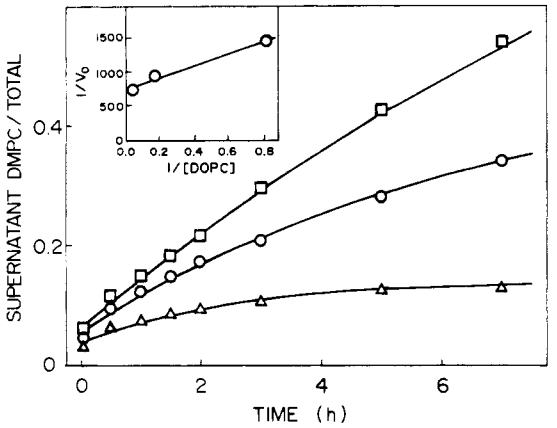

FIGURE 4: Transfer of [^{14}C]DMPC from erythrocytes (50% HCT) to DOPC vesicles. The fraction of [^{14}C]DMPC in the supernatant is shown as a function of time for prelabeled cells incubated with three concentrations of DOPC vesicles: 24.8 mmol/L of supernatant (□); 6.2 mmol/L of supernatant (○); 1.2 mmol/L of supernatant (△). The curves are nonlinear least-squares fits to the equation $y = a_0 + a_1[1 - \exp(-a_2 t)]$. Initial rates of lipid transfer (v_0) were taken from the fitted curves. Plotting $1/v_0$ vs. $1/[DOPC]$ yielded a straight line (inset). The y intercept of this line, determined by a linear least-squares fit, is 727 min, implying that $k_1 = (1.4 \pm 0.3) \times 10^{-3}$ min^{-1} (standard deviation, based upon two similar experiments).

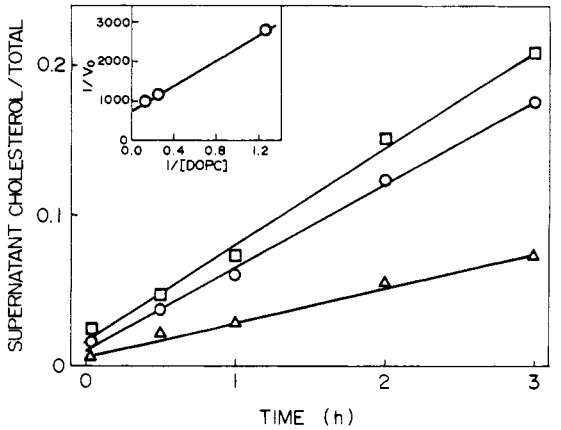

FIGURE 5: Transfer of cholesterol from erythrocytes (50% HCT) to DOPC vesicles. Supernatant cholesterol as a function of time for three concentrations of DOPC vesicles: 12.4 mmol/L of supernatant (□); 6.2 mmol/L of supernatant (○); 1.2 mmol/L of supernatant (△). Initial rates of cholesterol transfer (v_0) were taken from linear least-squares fits. Plotting $1/v_0$ vs. $1/[DOPC]$ yielded a straight line (inset). The y intercept, determined by linear least-squares fitting, is 702 min, implying that $k_1 = (1.4 \pm 0.3) \times 10^{-3}$ min^{-1}.

passive acceptors of transferable cell components (principally cholesterol and [^{14}C]DMPC; see below). As described in section B of the Appendix, the rate coefficient k_1 for the dissociation of [^{14}C]DMPC from the cells can be deduced from a plot of 1/(rate of transfer) vs. 1/(acceptor vesicle concentration). From the data in Figure 4, $k_1 = 1.4 \times 10^{-3}$ min^{-1}, compared with $(9.3 \pm 4.9) \times 10^{-3}$ min^{-1} for the dissociation of DMPC from vesicles.

Transfer of Cell Lipids to Vesicles. Assessment of the outer monolayer expansion resulting from cell incorporation of vesicle lipid would be complicated by any concurrent transfer of cell lipids to vesicles. This possibility was explored by incubating cells with DMPC or spin PC vesicles (464 μmol/L of supernatant, 50% HCT) and analyzing the lipids from cell-free supernatants by TLC. The only lipids detected were PC and cholesterol. To determine whether the PC contained any cell PC, cells were incubated with spin PC vesicles, and the supernatant lipid extracts were analyzed by reversed-phase TLC to separate spin PC from other PC. The only phospholipid detected was spin PC. Thus, under these conditions, cholesterol is the only cell lipid transferred to vesicles.

The transfer of cholesterol from cells to vesicles was explored by incubating erythrocytes with DOPC vesicles. The amount of cholesterol associated with the vesicles was measured as a function of time for three concentrations of acceptor vesicles and analyzed as described in part B of the Appendix. From the data in Figure 5, $k_1 = 1.4 \times 10^{-3}$ min^{-1}, in fair agreement with a published value, 3×10^{-3} min^{-1} (Lange et al., 1983). Cells incubated with DOPC at 12 mmol/L of supernatant, 50% HCT, lost about 20% of their cholesterol to the vesicles. Although cholesterol flip–flop is rapid (Lange et al., 1981), its transbilayer distribution favors the outer leaflet (Lange & Slayton, 1982), and its depletion turns discocytes into stomatocytes.

Cholesterol depletion was somewhat less extensive when cells were incubated with DMPC or spin PC vesicles; as vesicle lipid is transferred to the cells, fewer vesicles remain to accept cholesterol from the cells. To minimize the amount of cholesterol depletion in the shape change experiments described below, vesicle concentrations less than 500 μM and incubation times less than 90 min were used. Under these circumstances,

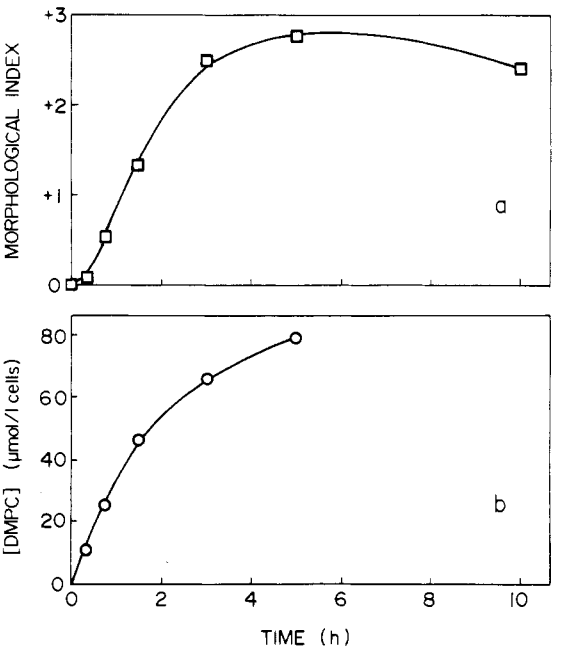

FIGURE 6: Morphological consequences of lipid transfer from vesicles to cells. (a) Morphological index as a function of time for erythrocytes (10% HCT) incubated with DMPC vesicles (28.7 μmol/L supernatant). (b) Lipid incorporation as a function of time for the same incubation.

less than 4% of the cells' cholesterol was transferred to the vesicles. This amount of cholesterol depletion has no measurable stomatocytogenic effect. Cholesterol depletion was avoided altogether in experiments using DLPC or egg lyso-PC, as the transfer of these lipids is much more rapid than cholesterol transfer.

Correlation between Lipid Incorporation and Shape Change. Erythrocytes were incubated with either spin PC, DMPC, DLPC, or egg lyso-PC, and their morphology was assessed by light microscopy. One such incubation, using DMPC vesicles, is shown in Figure 6. Lipid was transferred from the vesicles to the cells, which crenated in proportion to the amount of lipid incorporation. After crenation reached a plateau, the cells slowly reverted to the discoid form. This shape reversal had a half-time of roughly 22 h and persisted in the absence of exogenous lipid. The rates and extents of crenation, lipid

Table I: Calculated Differences between Outer and Inner Surface Areas of Model Echinocytes

θ (deg)	r_1 (nm)	s (nm)	t (nm)	n	R_{sphere} (μm)	ΔS (μm)^2	% ΔS
60	250	800	6	35	2.75	0.85	0.32
70	250	800	6	35	2.61	1.07	0.47
80	250	800	6	35	2.52	1.35	0.67
90	250	800	6	35	2.53	1.72	0.94
60	200	800	6	35	2.84	0.85	0.31
70	200	800	6	35	2.74	1.06	0.46
80	200	800	6	35	2.70	1.34	0.66
90	200	800	6	35	2.75	1.70	0.92
90	300	800	6	35	2.27	1.73	0.95
90	200	600	6	35	2.87	1.45	0.74
90	250	800	5	35	2.53	1.44	0.73
90	200	600	6	50	2.87	1.45	0.74
90	200	800	6	50	2.45	2.20	1.28
90	250	800	6	50	2.09	2.23	1.30
90	250	800	5	50	2.09	1.86	1.04
discocyte						0.41[a]	≡0
echinocyte stage 5 (smooth sphere)						0.42	0.01

[a] Taken from Beck (1978).

transfer, and shape recovery all decreased as the acyl chain length of the vesicle lipid increased.

The amount of lipid incorporated into the cells was determined by one of three procedures. Spin PC binding was measured by EPR spectroscopy. EPR spectra were taken of (1) the whole suspension, (2) the cell pellet, washed once in 150 mM NaCl, and (3) the supernatant. The amount of spin PC associated with the cells plus the amount in the supernatant always equalled the amount in a corresponding volume of whole suspension.

Binding of DMPC to cells was assessed by using [^{14}C]-DMPC as a tracer. At hematocrits of 10–50% and vesicle concentrations of 14–144 μmol/L of supernatant, DMPC incorporation approached a plateau after 5–8 h, with about 32% of the lipid taken up by the cells. For DLPC and egg lyso-PC, lipids were extracted from the supernatants after various time intervals and analyzed by TLC. No DLPC or egg lyso-PC remained in the supernatant after 10 min of incubation, suggesting that the lipid was incorporated quantitatively into the cells.

Clear correlations emerged between the amount of exogenous lipid transferred to the cells and the resulting cell shape (Figure 7) irrespective of hematocrit, initial lipid concentration, or length of incubation (at least for times that were short compared to the time scale of shape reversal; see Figure 6). On a molar basis, lyso-PC incorporation produced less shape change than diacyl-PC. About 85 μmol of exogenous PC/L of cells (4×10^6 molecules/cell) or 130 μmol of exogenous lyso-PC/L of cells (7×10^6 molecules/cell) yielded stage 3 echinocytes. Stage 4 echinocytes were produced by 120 μmol of PC/L of cells (6×10^6 molecules/cell) or 180 μmol of lyso-PC/L of cells (9×10^6 molecules/cell). ATP-depleted discocytes (produced by preincubation for 30 min in NaCl/P_i containing 10 mM inosine and 6 mM iodoacetamide) were no more or less sensitive to lipid treatment than were ATP-replete cells.

Theoretical Results. The formulas derived in part A of the Appendix were used to calculate the inner and outer surface areas of model echinocytes. The calculated bilayer imbalance depended roughly linearly on t (the thickness of the bilayer), s (the length of the shaft of the spike), and n (the number of spikes per cell) but was more sensitive to the choice of θ (Table I). The bilayer imbalance varied little with the choice of r_1 or r_2. Stage 3 echinocytes typically possess 35 spikes with $s \simeq 800$ nm, $r_1 \simeq r_2 \simeq 250$ nm, and $\theta \simeq 70$–90°. When these parameters are used, the echinocytes are calculated to have

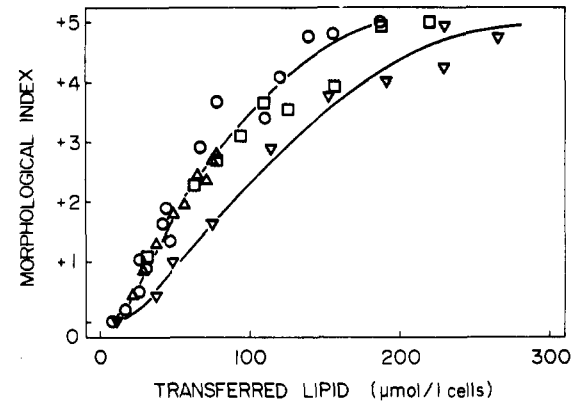

FIGURE 7: Erythrocyte shape as a function of lipid incorporation. Cells were incubated with egg lyso-PC (▽), DLPC (□), DMPC (○), or spin PC (△). Egg lyso-PC-induced crenation reached a maximum within a few seconds. This plateau level of crenation was shown to correspond to 100% incorporation of the egg lyso-PC. DLPC-loaded cells crenated maximally in about 5 min. It was assumed that 100% of the DLPC was then incorporated into the cells. DMPC incorporation was measured with [^{14}C]DMPC. Spin PC incorporation was determined from double integration of EPR spectra of the cell pellets.

0.4–0.9% more outer surface area than discocytes. Stage 4 echinocytes have about 50 spikes with $\theta \simeq 90°$, which corresponds to an expansion of the outer monolayer of 0.6–1.3%. This degree of outer monolayer expansion would appear to be as much as the intact erythrocyte can accommodate. During the conversion of stage 4 to stage echinocytes, the spikes break off to form membrane buds. Because of their small radius (about 50 nm), buds have a higher ratio of outer to inner leaflet than do cells. Thus, budding shrinks the outer monolayer more than the inner monolayer, relieving the bilayer imbalance. As Beck (1978) has pointed out, discocytes and stage 5 echinocytes have the same bilayer balance; they differ only in their volumes. We can use this observation to estimate the amount of budding that would convert a stage 4 echinocyte to stage 5. Each bud contains an excess of $4\pi(r_0^2 - r_i^2) = 5.97 \times 10^{-3}$ μm^2 outer surface area. The difference in outer monolayer area between a stage 4 echinocyte and a smooth sphere is roughly 0.9% or 1.26 μm^2. Thus, each cell should lose 210 buds, containing a total of 4.8% of its membrane. This prediction is in good agreement with experimental estimates (Ott et al., 1981; K.-J. Lee and W. H. Huestis, unpublished results).

Discussion

The data presented in Figures 2–4 show that spin PC and

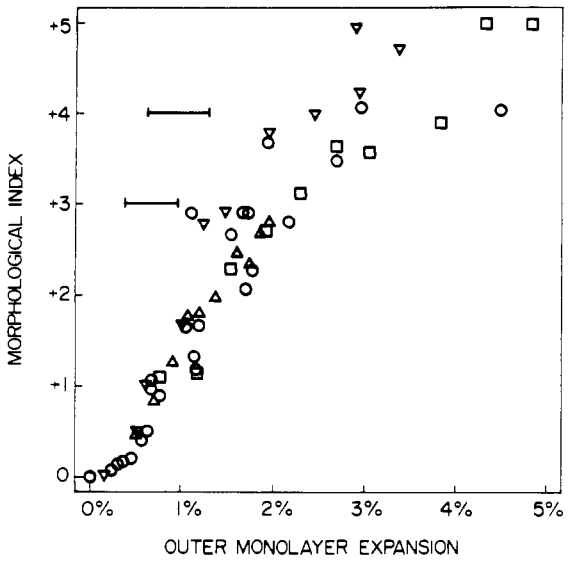

FIGURE 8: Relationship between erythrocyte shape and expansion of the membrane outer leaflet. Cells were loaded with egg lyso-PC (△), DLPC (□), DMPC (○), and spin PC (△). The horizontal bars represent the calculated outer monolayer expansions for model stage 3 and stage 4 echinocytes.

DMPC intercalate into the membranes of intact erythrocytes. The EPR spectrum of the cells after incubation with spin PC vesicles is the expected anisotropic triplet, not an isotropic triplet (expected if lipid monomers loosely adhere to the cells) or a broad singlet (expected if intact vesicles adhere to the cells). Erythrocytes do not take up the nontransferable marker cholesteryl oleate from DMPC vesicles, as would be expected if whole vesicles or vesicle fragments were adsorbed to the cells. Further, cell-associated DMPC resembles membrane-bound DMPC in its dissociation kinetics, showing slow transfer from cells to DOPC vesicles. These findings do not support the proposal that intact erythrocyte membranes have a high internal pressure that prevents intercalation of amphipaths (Conrad & Singer, 1981).

Several previous studies have estimated the amount of outer monolayer expansion needed to induce crenation. On the basis of geometrical models of echinocyte spikes, Beck (1978) suggested that as little as 0.4% expansion of the outer monolayer (or contraction of the inner monolayer) could convert discocytes to echinocytes. However, experimental studies implied that an order of magnitude more expansion is necessary (Matayoshi, 1980; Lovrien & Anderson, 1982). One notable exception was the recent report of Lange & Slayton (1982) in which about 1–1.5% expansion of the outer monolayer was estimated to produce echinocytes (stage of crenation not specified).

Our calculations predict that 0.4–0.9% expansion of the outer monolayer of a discocyte should yield a stage 3 echinocyte and that 0.6–1.3% expansion corresponds to stage 4 morphology. These estimates are in good agreement with Beck's previous calculation which was based on a model with conical (instead of rounded) spikes.

The lipid binding data presented in Figure 7 can be used to test these calculations. To relate the amount of exogenous lipid incorporated to outer leaflet expansion, we need to know the area occupied by a molecule of each type of lipid. On the basis of several X-ray diffraction studies of saturated diacyl-PC in fully hydrated model membranes [summarized by Cornell & Separovic (1983)], it is estimated that PC occupies 0.65 nm^2/molecule. Egg lyso-PC has been estimated to occupy 0.34 ± 0.13 nm^2/molecule (Lange & Slayton, 1982).

Using these estimates, we can determine the amount of outer monolayer expansion in lipid-treated cells. As shown in Figure 8, stage 3 echinocytes result from a 1.7% ± 0.6% expansion of the outer leaflet, and stage 4 echinocytes result from a 2.7% ± 1.1% expansion. These experimental estimates agree with the calculations to within a factor of about 2. The experimental estimates might be too high for four reasons. First, if the shape recovery (shown for DMPC in Figure 6) arises from lipid flip-flop, then the assumption that all the loaded lipid resides in the outer monolayer would be incorrect. Second, cholesterol depletion partially offsets the effects of DMPC and spin PC loading. Third, it is possible that some of the cell-associated lyso-PC and DLPC are not intercalated into the membrane, although by analogy to DMPC and spin PC this amount is not likely to be very large. Finally, homeostatic mechanisms might expand the inner monolayer in response to the expanded outer monolayer (Alhanaty & Sheetz, 1981).

Our previous estimate of the amount of inner monolayer contraction (roughly 0.65%) that accompanies metabolic crenation (to MI = +3) is in reasonable agreement with the theoretical and experimental estimates of the amount of lipid loading required to produce the same shape change. This observation supports the hypothesis (Ferrell & Huestis, 1984) that metabolic crenation arises from bilayer imbalance caused by phosphatidylinositol 4,5-bisphosphate and phosphatidic acid degradation and corroborates the assertion (Lange et al., 1982) that erythrocyte shape changes can be explained in the context of the bilayer couple hypothesis without invoking rearrangements of the erythrocyte cytoskeleton.

ACKNOWLEDGMENTS

We thank Alexandra Newton for help with nonlinear least-squares curve fitting and Hoai-Thu Truong for help with the calculations in part A of the Appendix.

APPENDIX

(*A*) *Geometrical Models of Echinocyte Spikes.* Scanning electron microscopy shows that echinocyte spikes are cylindrical or conical, with rounded tips and bases. In stage 3–5 echinocytes, the spikes rest on a roughly spherical surface. In this section, formulas are derived for the inner and outer surface areas of such echinocytes.

As shown in Figure 9, five variables define the geometry of the echinocyte spike: r_1, the radius of curvature of the tip; r_2, the radius of curvature of the base; s, the length of the shaft; θ, the angle of inclination of the shaft; and t, the thickness of the membrane.

The tip of the spike is part of a sphere whose surface area is $S = 2\pi r^2(1 - \cos\theta)$ where r is the radius of curvature of the sphere. For the outer leaflet, $r = r_1$; for the inner leaflet, $r = r_1 - t$. Thus, the outer surface area of the tip of the spike is

$$S = 2\pi r_1^2(1 - \cos\theta) \quad \text{(A1)}$$

and the difference between the outer and inner surface areas is

$$\Delta S = 2\pi(2r_1t - t^2)(1 - \cos\theta) \quad \text{(A2)}$$

The surface area of the conical shaft is given by $S = \pi s(R_1 + R_2)$ where $R_1 = r_1 \sin\theta$ and $R_2 = r_1 \sin\theta + s\cos\theta$ for the outer leaflet and $R_1 = (r_1 - t)\sin\theta$ and $R_2 = (r_1 - t)\sin\theta + s\cos\theta$ for the inner leaflet. The area of the outer surface is given by

$$S = \pi s(2r_1 \sin\theta + s\cos\theta) \quad \text{(A3)}$$

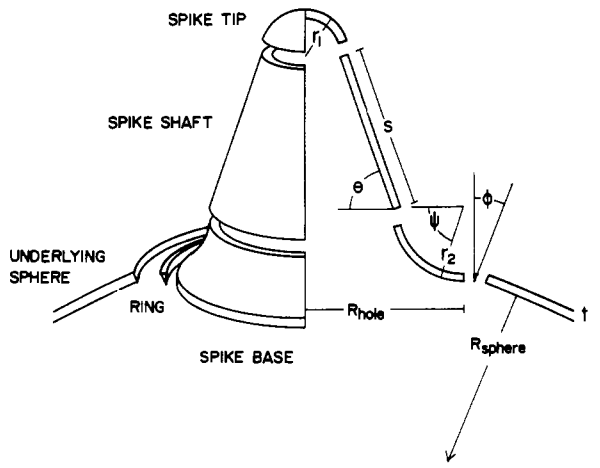

FIGURE 9: Geometrical model of an echinocyte spike. The five sections of the model spike are illustrated on the left. Parameters used in calculating inner and outer surface areas are shown on the right. The cell geometry is determined by r_1 (the radius of the tip of the spike), r_2 (the radius of the base of the spike), s (the length of the shaft of the spike), θ (the inclination of the shaft of the spike), t (the thickness of the membrane, and n (the number of spikes per cell). The other parameters shown [R_{hole} (the radius of the base of the spike), R_{sphere} (the radius of the underlying sphere), and ϕ (the angle at which the spike joins the sphere)] can all be deduced from the first five parameters and the known surface area of an erythrocyte. ψ is an angular coordinate used in calculating the surface area of the base of the spike.

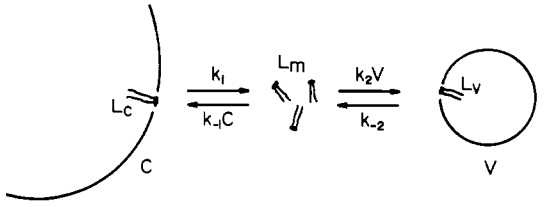

FIGURE 10: Kinetic model for transfer of [^{14}C]DMPC and cholesterol from erythrocytes to DOPC vesicles. C, cells; L_c, the DMPC or cholesterol in the cells; L_m, the monomeric DMPC or cholesterol; V, the DOPC vesicles; L_v, the DMPC or cholesterol in the vesicles.

and the difference between the areas of the leaflets is

$$\Delta S = 2\pi st \sin\theta \tag{A4}$$

The base of the spike is a more complicated geometrical form, the surface of revolution of a circular arc. It is convenient to express the radius of this torus and the infinitesimal arc length of the circle in terms of the angle ψ, defined in Figure 9. The surface area of the torus becomes

$$S = 2\pi \int_{\pi/2-\theta}^{\pi/2} r(\psi)\rho \, d\psi \tag{A5}$$

where $\rho = r_2$ for the outer leaflet and $r_2 + t$ for the inner leaflet. The choice of $\psi = \pi/2$ as the upper limit of integration assumes that the spike is joined to a flat surface, whereas actually it joins a sphere at an angle ϕ. This discrepancy will be considered later.

For the outer monolayer, $r(\psi) = R_{hole} - r_2 \cos\psi$, where $R_{hole} = r_1 \sin\theta + s\cos\theta + r_2 \sin\theta$; for the inner monolayer, $r(\psi) = R_{hole} - (r_2 + t)\cos\psi$. After evaluating the integral and using the identity $\sin(\pi/2 - \theta) = \cos\theta$, we find that the area of the outer surface is

$$S = 2\pi r_2[\theta(r_1 \sin\theta + s\cos\theta + r_2 \sin\theta) - r_2(1 - \cos\theta)] \tag{A6}$$

and

$$\Delta S = -2\pi t\theta(r_1 \sin\theta + s\cos\theta + r_2 \sin\theta) + 2\pi(2r_2 t + t^2)(1 - \cos\theta) \tag{A7}$$

In total, the outer surface area of a spike (from eq A1, A3, and A6) is

$$S_{spike} = 2\pi(r_1^2 - r_2^2)(1 - \cos\theta) + \pi s(2r_1 \sin\theta + s\cos\theta) + 2\pi r_2\theta[(r_1 + r_2)\sin\theta + s\cos\theta] \tag{A8}$$

and the difference between the outer and inner surface areas (eq A2, A4, and A7) is

$$\Delta S_{spike} = 4\pi t(r_1 + r_2)(1 - \cos\theta) + 2\pi st \sin\theta - 2\pi t\theta[(r_1 + r_2)\sin\theta + s\cos\theta] \tag{A9}$$

The spikes rest on an underlying sphere that resembles a whiffle ball, with holes at the bases of the spikes. The membrane portions of the sphere contribute different amounts of surface area to the inner and outer monolayers. The two parameters that define the geometry of the sphere and its attachments to the spikes are R_{sphere}, its radius, and ϕ, the angle at which the spikes join the sphere. The values of these variables can be derived from S_{spike}, the number of spikes n, and the known total surface area of the cell.

The holes contribute approximately

$$S = n\pi R_{hole}^2 = n\pi[(r_1 + r_2)\sin\theta + s\cos\theta]^2 \tag{A10}$$

to S_{sphere}, the outer surface of the sphere; the membrane portions contribute $S = S_{cell} - nS_{spike}$, where $S_{cell} = 140\ \mu m^2$ (Wintrobe, 1981). Thus

$$S_{sphere} = S_{cell} - nS_{spike} + n\pi[(r_1 + r_2)\sin\theta + s\cos\theta]^2 \tag{A11}$$

and

$$R_{sphere} = (S_{sphere}/4\pi)^{1/2} \tag{A12}$$

It follows that the difference between the outer and inner surfaces areas of the membrane portions of this sphere is

$$\Delta S_{sphere} = [(S_{cell} - nS_{spike})/S_{sphere}][4\pi(2R_{sphere}t - t^2)] \tag{A13}$$

Finally, there is an annulus of outer monlayer area where each spike joins the underlying sphere. The surface area of each annulus is given by

$$\Delta S_{annulus} = 2\pi[R_{hole}t\phi + t^2(1 - \cos\phi)] \tag{A14}$$

where ϕ is the angle at which the base of the spike joins the underlying sphere (Figure 9) and

$$\phi = \sin^{-1} R_{hole}/R_{sphere} \tag{A15}$$

Thus, the total bilayer imbalance of the echinocyte has three contributions: from the spikes (eq A9), from the underlying sphere (eq A13), and from rings of outer monolayer where the spikes join the sphere (eq A14).

(B) Kinetics of Lipid Exchange between Cells and DOPC Vesicles. The results in the following paper (Ferrell et al., 1985) along with several other reports (Martin & MacDonald, 1976; Roseman & Thompson, 1980; Backer & Dawdowicz, 1981; Nichols & Pagano, 1981; McLean & Phillips, 1981) suggest that transfer of cholesterol or DMPC from cells to vesicles is at least a two-step process. The rate-limiting step is the dissociation of a monomer of lipid from the cell into the supernatant, the rate of which is directly related to the lipid's hydrophilicity (Ferrell et al., 1985). The monomer can then collide with and be incorporated into a vesicle (Figure 10). In this section, we derive an expression for analyzing the transfer of relatively hydrophilic lipids (like cholesterol or

DMPC) between cells and vesicles composed of relatively hydrophobic or "nontransferable" lipid (like DOPC).

Lipid transfer is monitored by the appearance of the lipid L in the vesicle fraction. The rate of lipid transfer is described by

$$\frac{dL_v}{dt} = k_2 L_m V - k_{-2} L_v \quad \text{(B1)}$$

where L_v is the concentration of L in the vesicle fraction, L_m is the monomeric lipid concentration, and V is the concentration of the acceptor vesicles. All concentrations are expressed as moles per liter of supernatant.

The rate of appearance of L_m is

$$\frac{dL_m}{dt} = k_1 L_c + k_{-2} L_v - (k_{-1} C + k_2 V) L_m \quad \text{(B2)}$$

where L_c is the concentration of L in the cells and C is the concentration of cell (donor) membranes. Assuming that L_m quickly reaches a steady state, it follows that

$$\frac{dL_m}{dt} = 0 \quad \text{(B3)}$$

$$L_m = \frac{k_1 L_c + k_{-2} L_v}{k_{-1} C + k_2 V} \quad \text{(B4)}$$

Substituting $L_{tot} - L_v - L_m$ for L_c yields

$$L_m = \frac{k_1 L_{tot} - (k_1 - k_{-2}) L_v}{k_1 + k_{-1} C + k_2 V} \quad \text{(B5)}$$

$$\frac{dL_v}{dt} = \frac{k_1 k_2 V L_{tot} - (k_1 k_{-2} + k_1 k_2 V + k_{-1} k_{-2} C) L_v}{k_1 + k_{-1} C + k_2 V} \quad \text{(B6)}$$

We can simplify this expression by momentarily considering the special case of equilibrium, when

$$\frac{dL_v}{dt} = 0 \quad \text{(B7)}$$

It follows from eq B6 that

$$(L_v)_{eq} = \frac{k_1 k_2 V L_{tot}}{k_1 k_{-2} + k_1 k_2 V + k_{-1} k_{-2} C} \quad \text{(B8)}$$

This definition can be inserted into eq B6, which becomes

$$\frac{dL_v}{dt} = \frac{d[L_v - (L_v)_{eq}]}{dt} = - \frac{k_1 k_{-2} + k_1 k_2 V + k_{-1} k_{-2} C}{k_1 + k_{-1} C + k_2 V} [L_v - (L_v)_{eq}] \quad \text{(B9)}$$

Hence, lipid transfer is first order in $L_v - (L_v)_{eq}$ with an apparent rate coefficient

$$k_{app} = \frac{k_1 k_{-2} + k_1 k_2 V + k_{-1} k_{-2} C}{k_1 + k_{-1} C + k_2 V} \quad \text{(B10)}$$

An expression for $v_o = (dL_v/dt)_{t=0}$ as a function of V and C follows also from eq B6:

$$v_o = \frac{k_1 k_2 V L_{tot}}{k_1 + k_{-1} C + k_2 V} \quad \text{(B11)}$$

In double-reciprocal form:

$$\frac{1}{v_o} = \left(\frac{1}{k_2} + \frac{k_{-1} C}{k_1 k_2} \right) \frac{1}{V} + \frac{1}{k_1} \quad \text{(B12)}$$

Thus, k_1, the rate coefficient for dissociation of a lipid monomer from a cell, can be deduced from the intercept of a plot of $1/v_o$ vs. $1/V$. Equation B12 is well fit by the data in Figures 4 and 5.

Registry No. DLPC, 18285-71-7; DMPC, 13699-48-4; DOPC, 10015-85-7; 1-palmitoyl-2-stearoylphosphatidylcholine, 10589-47-6; cholesterol, 57-88-5.

REFERENCES

Alhanaty, E., & Sheetz, M. P. (1981) *J. Cell Biol. 91*, 884–888.

Allan, D., & Michell, R. H. (1978) *Biochim. Biophys. Acta 508*, 277–286.

Allan, D., & Thomas, P. (1981) *Biochem. J. 198*, 433–440.

Allan, D., Watts, R., & Michell, R. H. (1976) *Biochem. J. 156*, 225–232.

Allan, D., Thomas, P., & Michell, R. H. (1978) *Nature (London) 276*, 289–290.

Backer, J. M., & Dawidowicz, E. A. (1981) *Biochemistry 20*, 3805–3810.

Beck, J. S. (1978) *J. Theor. Biol. 75*, 487–501.

Bessis, M. (1973) in *Red Cell Shape* (Bessis. M., Weed, R. I., & LeBlond, P. F., Eds.) pp 1–23, Springer-Verlag, New York.

Bouma, S. R., Drislane, F. W., & Huestis, W. H. (1977) *J. Biol. Chem. 252*, 6759–6763.

Chalpin, D. B., & Kleinfeld, A. M. (1983) *Biochim. Biophys. Acta 731*, 465–474.

Conrad, M. J., & Singer, S. J. (1981) *Biochemistry 20*, 808–818.

Cornell, B. A., & Separovic, F. (1983) *Biochim. Biophys. Acta 733*, 189–193.

DeCuyper, M., Joniau, M., & Dangreau, H. (1983) *Biochemistry 22*, 415–420.

Devaux, P., Scandella, C. J., & McConnell, H. M. (1973) *J. Magn. Reson. 9*, 474–485.

Ferrell, J. E., Jr., & Huestis, H. W. (1984) *J. Cell Biol. 98*, 1992–1998.

Ferrell, J. E., Jr., Lee, K.-J., & Huestis, W. H. (1985) *Biochemistry* (following paper in this issue).

Fujii, T., Sato, T., Tamura, A., Wakatsuki, M., & Kanaho, Y. (1979) *Biochem. Pharmacol. 28*, 613–620.

Lange, Y., & Slayton, J. (1982) *J. Lipid Res. 23*, 1121–1127.

Lange, Y., Dolde, J., & Steck, T. L. (1981) *J. Biol. Chem. 256*, 5321–5323.

Lange, Y., Hadesman, R. A., & Steck, T. L. (1982) *J. Cell Biol. 92*, 714–721.

Lange, Y., Molinaro, A. L., Chauncey, T. R., & Steck, T. L. (1983) *J. Biol. Chem. 258*, 6920–6926.

Lew, V. L. (1971) *Biochim. Biophys. Acta 233*, 827–830.

Lovrien, R., & Anderson, R. A. (1982) *Biophys. J. 37*, 12–14.

Martin, F. J., & MacDonald, R. C. (1976) *Biochemistry 15*, 321–327.

Matayoshi, E. D. (1980) *Biochemistry 19*, 3414–3422.

McLean, L. R., & Phillips, M. C. (1981) *Biochemistry 20*, 2893–2900.

Mohandas, M., Wyatt, J., Mel, S. F., Rossi, M. E., & Shohet, S. B. (1982) *J. Biol. Chem. 257*, 6537–6543.

Nakao, M., Nakao, T., & Yamazoe, S. (1960) *Nature (London) 187*, 945–946.

Nichols, J. W., & Pagano, R. E. (1981) *Biochemistry 20*, 2783–2789.

Ott, P., Hope, M. J., Verkleij, A. J., Roelofsen, B., Brodbeck, U., & van Deenen, L. L. M. (1981) *Biochim. Biophys. Acta 641*, 79–87.

Roseman, M. A., & Thompson, T. E. (1980) *Biochemistry 19*, 439–444.

Sheetz, M. P., & Singer, S. J. (1974) *Proc. Natl. Acad. Sci. U.S.A. 71*, 4457–4461.
Stockton, G. W., Polnaszek, C. F., Leitch, L. C., Tulloch, A. P., & Smith, I. C. P. (1974) *Biochem. Biophys. Res. Commun. 60*, 844–850.
White, J. G. (1974) *Am. J. Pathol. 77*, 507–518.
Wintrobe, M. M. (1981) *Clinical Hematology*, 8th ed., Lea & Febiger, Philadelphia, PA.
Zlatkis, A., Zak, B., & Boyle, A. J. (1953) *J. Lab. Clin. Med. 41*, 486–492.

Lipid Transfer between Phosphatidylcholine Vesicles and Human Erythrocytes: Exponential Decrease in Rate with Increasing Acyl Chain Length†

James E. Ferrell, Jr., Kong-Joo Lee, and Wray H. Huestis*
Department of Chemistry, Stanford University, Stanford, California 94305
Received June 18, 1984; Revised Manuscript Received November 6, 1984

ABSTRACT: The rate of phospholipid transfer from sonicated phospholipid vesicles to human erythrocytes has been studied as a function of membrane concentration and lipid acyl chain composition. Phospholipid transfer exhibits saturable first-order kinetics with respect to both cell and vesicle membrane concentrations. This kinetic behavior is consistent either with transfer during transient contact between cell and vesicle surfaces (but only if the fraction of the cell surface susceptible to such interaction is small) or with transfer of monomers through the aqueous phase. The acyl chain composition of the transferred phospholipid affects the transfer kinetics profoundly; for homologous saturated phosphatidylcholines, the rate of transfer decreases exponentially with increasing acyl chain length. This behavior is consistent with passage of phospholipid monomers through a polar phase, which might be the bulk aqueous phase (as in the monomer transfer model) or the hydrated head-group regions of a cell–vesicle complex (transient collision model). Collisional transfer also predicts that intercell transfer of phospholipids should be slow compared to cell–vesicle transfer, as surface charge and steric effects should prevent close apposition of donor and acceptor membranes. This is not found; dilauroylphosphatidylcholine transfers rapidly between red cells. Thus, the observed relationship between acyl chain length and intermembrane phospholipid transfer rates likely reflects the energetics of monomer transfer through the aqueous phase.

In the preceding paper (Ferrell et al., 1985), phospholipid transfer from synthetic vesicles to human erythrocytes served as a convenient method for changing the bilayer balance of the erythrocyte membrane. However, lipid transfer is a phenomenon of broader theoretical and practical interest, being of central importance for an understanding of membrane lipid dynamics.

Two types of mechanisms have been proposed for the spontaneous transfer of lipids between biological membranes (Figure 1). The first involves lipid transfer during transient collisions between the donor and acceptor membranes. In the second, lipid monomers dissociate from the donor membrane, diffuse through the aqueous phase, and associate with the acceptor membrane. Evidence from several laboratories favors the second model for the transfer of phospholipids and cholesterol between a variety of donors and acceptors (Martin & MacDonald, 1976; Duckwitz-Peterlein et al., 1977; Roseman & Thompson, 1980; Nichols & Pagano, 1981; Backer & Dawidowicz, 1981; McLean & Phillips, 1981; Massey et al., 1982; DeCuyper et al., 1983; Lange et al., 1983), although other evidence supports the collision model (Martin & MacDonald, 1976; Kremer et al., 1977).

It is frequently argued that the kinetics of lipid transfer can distinguish between these two models, supposing the rate of transfer to be first order in both donor and acceptor membrane concentrations in the collision model and first order in donor concentration alone in the monomer transfer model. As the following discussion will show, this distinction is valid only for limiting cases. In general, initial transfer rates depend on donor and acceptor concentrations in a saturable (hyperbolic) fashion in both models. The kinetic data that have been garnered in support of monomer transfer do not rule out the transient collision model.

Given this ambiguity, further tests are required to distinguish between the two models. The collision model can be evaluated by altering the physical properties of the donor and acceptor membranes in ways that discourage formation of complexes. The monomer transfer model can be tested by examining a prediction which follows from simple thermodynamic arguments. The dissociation of a lipid monomer into the aqueous phase would increase the ordering of the water molecules that contact its acyl chains. The free energy of this process should be directly proportional to the length of the chains (Tanford, 1980). The Hammond postulate (March, 1977) predicts that the transition state of a dissociating lipid would resemble a free monomer. Thus, the free energy of activation would also be roughly proportional to the length of the acyl chains, and the rate of lipid transfer would decrease sharply as acyl chain length increased. In particular, the rate coefficient for monomer dissociation (k_1 in Figure 1c) would decrease exponentially with increasing chain length. In the present study, we measured the kinetics of transfer of five

† This work was supported by grants from the National Institutes of Health (HL 23787) and the American Heart Association (Grant in Aid 80990).

0006-2960/85/0424-2857$01.50/0